THE SIGNIFICANCE OF THE REDOX STATE OF GLASS FOR THE BUBBLE BEHAVIOUR AT NON-ISOTHERMAL CONDITIONS

LUBOMÍR NĚMEC, MARKÉTA RAKOVÁ

Laboratory of Inorganic Materials of IIC ASCR and ICT, Technická 5, 166 28 Prague

Received September 2, 1997.

The model of calculation of the simultaneous oxidation-reduction equilibria in non-isothermal flowing glass melt has been formulated. The behaviour of bubbles in a model glass melting furnace has been examined using this model. The calculations involved soda-lime-silica glass containing sulphate ions and ions of iron as well as glass for the production TV panels with antimony and cerium. The results of calculations confirmed results acquired under isothermal conditions. The internal partial pressure of the refining gas, the bubble growth rate and the refining rate grew with the increasing initial redox state of glass in the glass for TV panels. In the glass containing sulphate ions, the driving force of refining (the sum of the internal partial pressures of SO_2 and O_2 in the melt) exhibited minimum at the medium values of the initial redox, so the bubble growth rate and the refining rate were highest either at very high or very low values of the initial redox state of glass. The coupled mathematical model of the redox state calculation and bubble behaviour has been used to calculate the final bubble properties for two bubble sources: glass batch and air coming from the furnace refractory materials.

INTRODUCTION

The model of multicomponent bubble behaviour at isothermal conditions was presented in [1], taking into account the actual redox state of glass. Its numerical solution was applied to the examination of influence of the initial redox state of glass on the refining behaviour of two industrial glasses: float glass and glass for the production of TV panels. The results of calculations have shown that the initial redox state of glass had an impact both on the rate of bubble removing from glass and final properties of bubbles, currently used for the identification of bubble sources in glass melting furnaces. The calculations of internal partial pressures of refining gases in the glass made it possible to define conditions of potential bubble nucleation. The mentioned results have practical importance for the industrial glass melting process, however, the bubble description must be adjusted to real conditions of the non-isothermal flowing glass in a glass melting space. The boundary conditions of real glass melting must be considered too.

This work presents the model of bubble behaviour considering the distribution of oxidation-reduction species in the model glass melting space. Soda-lime-silica glass containing iron ions and sulphates as well as glass for TV panels containing ions of antimony and cerium were applied for the model calculations. In both glasses, the behaviour of bubbles coming from the glass batch layer was examined at different levels of the initial redox state of glass. The potential bubble nucleation regions in the furnace were defined. The ability of the model to use its results for the identification of bubble sources in a glass melting furnace was demonstrated in the second part of the work.

THEORETICAL PART

The set of equations describing the multicomponent bubble behaviour at isothermal conditions was presented in [1]. At non-isothermal conditions, equation (2) in [1] has an additional term expressing the influence of temperature variations. The complete form is then:

$$\frac{dp_i}{d\tau} = \frac{1.14\, RTD_i^{2/3} g^{1/3} \rho^{1/3}(m_{ib}-m_{ia})}{M_i \eta^{1/3} a} - \frac{3p_i}{a}\frac{da}{d\tau} + \frac{p_i}{T}\frac{dT}{d\tau} \quad , (1)$$

where p_i is the partial pressure of the i-th gas in the bubble, D_i is its diffusion coefficient in a glass melt, M_i its molecular weight, m_{ib} is its bulk concentration in the glass and m_{ia} its concentration on the bubble surface, a is bubble radius and ρ and η are glass density and viscosity, respectively.

For an individual multivalent element, Me_i, in a glass melt, the redox equilibrium reaction can be written as:

$$4/b_i\, Me_i^{(a_i+b_i)+}(l) + 2O^{2-}(l) \rightleftarrows 4/b_i\, Me_i^{a_i+}(l) + O_2(l,g) \quad .(2)$$

The simultaneous equilibrium of more oxidation-reduction pairs at isothermal conditions can be calculated following Theoretical part in [1]. Under non-isothermal conditions of flowing glass, the simultaneous equilibrium is shifted due to the mass transport of reaction components by glass convection and component diffusion through the melt. As a result, the new distribution of oxidation-reduction components will set up in the stationary state. The diffusion and convective equations

for the transport of components in equation (2) may be written as:

$$D_{Me_i}^{(a_i+b_i)+} \nabla^2 c_{Me_i}^{(a_i+b_i)+} - v\nabla c_{Me_i}^{(a_i+b_i)+} + \omega_{Me_i}^{(a_i+b_i)+} = 0 \quad , \tag{3}$$

$$D_{Me_i}^{a_i+} \nabla^2 c_{Me_i}^{a_i+} - v\nabla c_{Me_i}^{a_i+} + \omega_{Me_i}^{a_i+} = 0 \quad , \tag{4}$$

$$D_{O_2} \nabla^2 c_{O_2} - v\nabla c_{O_2} + \omega_{O_2} = 0 \quad , \tag{5}$$

where ω_i is the rate of the concentration change of species brought about by the shifting of chemical equilibrium in the i-th oxidation-reduction reaction and v is the vector of glass melt velocity.

The unknown values of ω_i are bound by the reaction stoichiometry, for instance:

$$\omega_{Me_i}^{(a_i+b_i)+} = -\omega_{Me_i}^{a_i+} \quad . \tag{6}$$

The initial oxidation-reduction distribution of species is computed using the values of equilibrium constants, the temperature distribution in the melt at the initial given value of oxygen concentration and the initial concentrations of oxidation-reduction ions. Subsequently, the numerical solution of equations (3 - 6) follows and alternates with the calculation of the new chemical equilibrium till the stationary state is attained. The numerical computation program REDOX was developed to perform the mentioned calculations and used simultaneously with the program GLASS MODEL for the computation of glass temperatures and velocities in a glass melting furnace [2]. The values of the necessary constants were taken from literature [3] or measured in the Laboratory of Inorganic Materials [4].

RESULTS OF CALCULATION

To demonstrate the significance of the initial redox state of glass for the refining process in a model melting space, the trajectories of bubbles, the values of internal partial pressures of refining gases as well as temperatures along these trajectories, the refining times and the maximum x - coordinates of refined bubbles were followed. The model melting space was 15m long, 4m wide, with 1m thick layer of soda-lime-silica glass (74 wt.% SiO_2, 16 wt.% Na_2O, 10 wt.% CaO) refined by sodium sulphate or with glass for production of TV panels refined by antimony. The simultaneous equilibrium $S^{6+} \rightleftarrows S^{4+}$ and $Fe^{3+} \rightleftarrows Fe^{2+}$ was considered in the former case, the later involved $Sb^{5+} \rightleftarrows Sb^{3+}$ and $Ce^{4+} \rightleftarrows Ce^{3+}$. Figure 1 presents an example of bubble trajectories from two representative starting points of bubbles situated under batch blanket [x = 2.7; y = 2.2; z = 0.2] (m) and [x = 0.6; y = 2.2; z = 0.2] (m). The sums of partial pressures of $SO_2 + O_2$ in the starting points for both kinds of glasses are presented in Figure 2 showing the similar dependence on the initial redox state of glass as was already demonstrated in [1]. I.e. the average driving force of gas transport into bubbles in the sulphate refined glass has its minimum value at the medium level of the initial redox (despite the fact the average temperature plotted in Figure 3*a* exhibited its highest value just at these medium redox levels). When examining the antimony refined glass, the $p_{O_2\ melt}$ dependence versus the redox state of glass shows a monotonous increase in the case of the starting point [x = 2.7; y = 2.2; z = 0.2] (m). In the second starting point [0.6; 2.2; 0.2], the value of $p_{O_2\ melt}$ is too low to

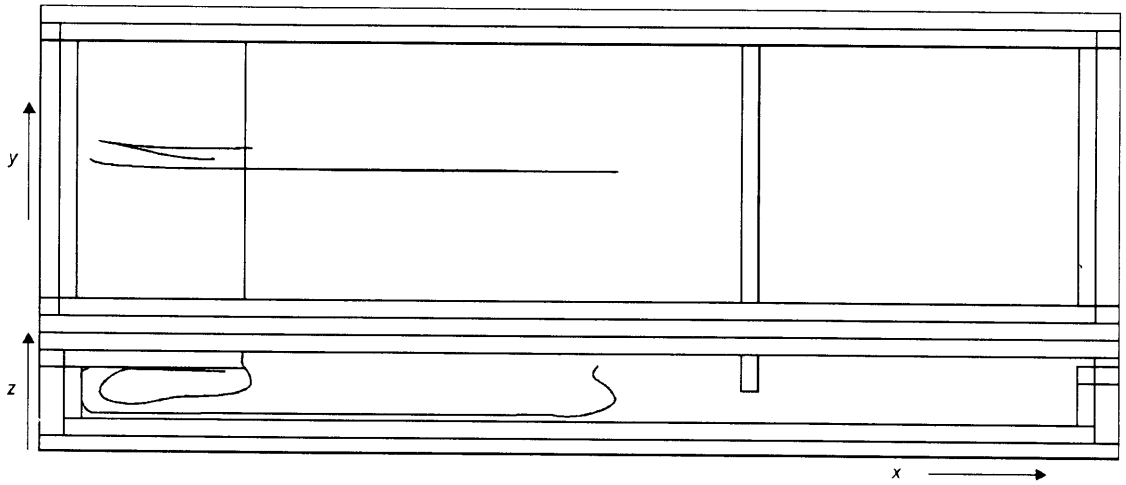

Figure 1. The XZ and XY projections of trajectories of bubbles coming from the glass batch into the model melting space and starting at x = 0.6; y = 2.2; z = 0.2 and x = 2.7; y = 2.2; z = 0.2 (m). The initial redox state of glass 0.1 mol.O_2 m^{-3} glass, a_0 = 0.1 (mm), c_{0CO_2} = 95 vol.%, c_{0N_2} = 5 vol.%. Glass for the production of TV panels.

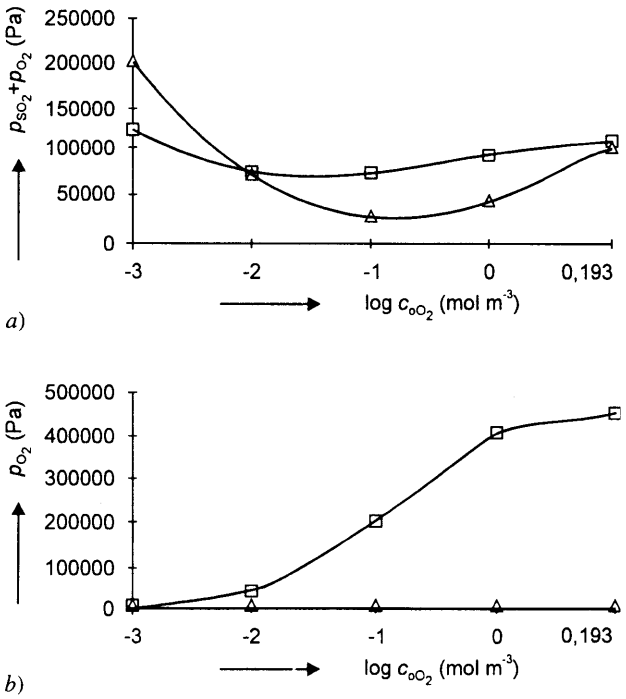

Figure 2. The internal partial pressures of refining gases in the starting points situated under batch blanket versus the initial redox state of glass. Δ - starting point 0.6; 2.2; 0.2] (m), □ - starting point [2.7; 2.2; 0.2] (m)
a) soda-lime-silica glass refined by sulphate
b) TV glass refined by antimony

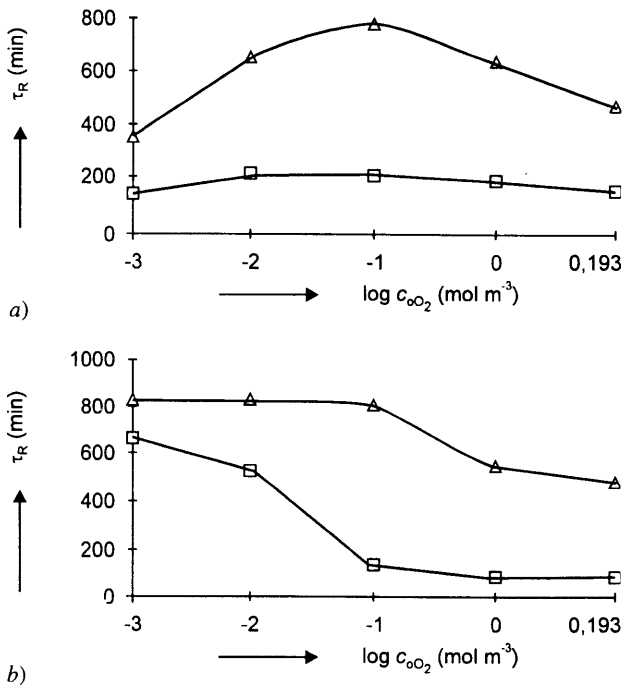

Figure 4. The refining times of the bubble having the initial radius a_0 = 0.1 mm, and initial composition c_{oCO_2} = 95 vol.%, c_{oN_2} = 5 vol.%, as a function of the initial redox state of glass. Δ - starting point 0.6; 2.2; 0.2] (m), □ - starting point [2.7; 2.2; 0.2] (m)
a) soda-lime-silica glass refined by sulphate
b) TV glass refined by antimony

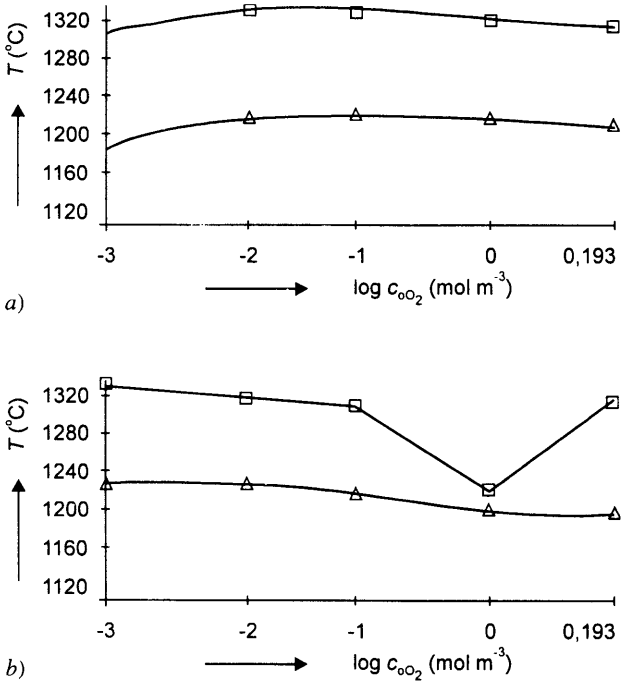

Figure 3. The average temperature along two representative bubble trajectories in the soda-lime-silica glass in dependence on the initial redox state of glass.
a) soda-lime-silica glass refined by sulphate
b) TV glass refined by antimony

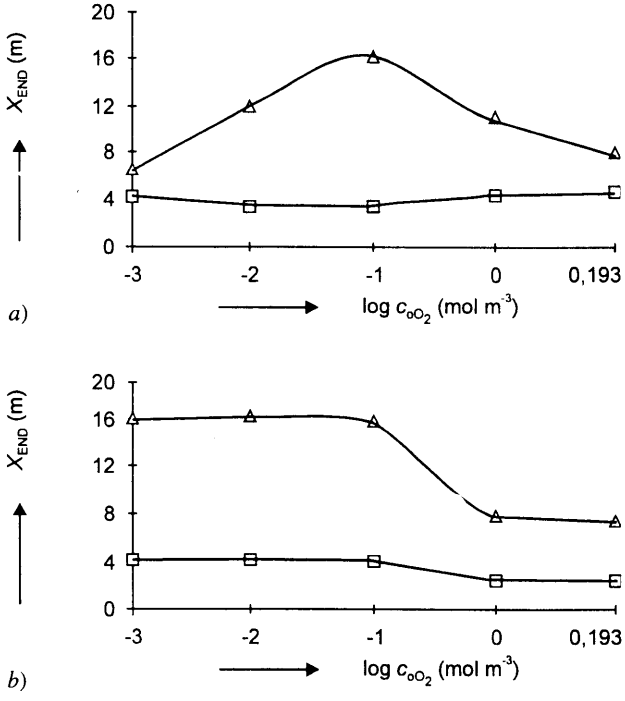

Figure 5. The x-coordinate of the bubble when reaching the glass level, x_{end}, as a function of the initial redox state of glass, a_0 = 0.1 mm, c_{oCO_2} = 95 vol.%, c_{oN_2} = 5 vol.%. Δ - starting point 0.6; 2.2; 0.2] (m), □ - starting point [2.7; 2.2; 0.2] (m)
a) soda-lime-silica glass refined by sulphate
b) TV glass refined by antimony

reveal the similar tendency (see figure 2*b*). This tendency must be however valid for the average values of $p_{O_2\,melt}$ along the bubble trajectory. The rate of the refining process can be expressed by the behaviour of single bubbles as is obvious from figure 4. The increasing driving force of gas transport into bubbles projects into the shorter refining times of bubbles, τ_R, and in most cases as well into their shorter final x - co-ordinates of bubble bursting on the glass level, as is obvious form figure 5. The final composition of bubbles at final temperature, being not too far from the stationary state in the soda-lime-silica glass, exhibits an increasing CO_2/N_2 ratio with increasing driving force of gas transport too. This fact brings figure 6.

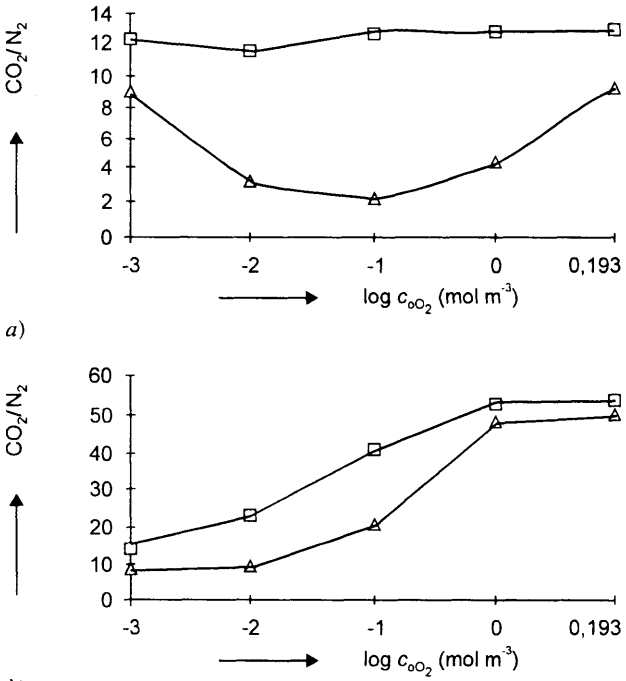

Figure 6. The final CO_2/N_2 concentration ratio in the refined bubbles as a function of the initial redox state of glass.
Δ - starting point 0.6; 2.2; 0.2] (m), □ - starting point [2.7; 2.2; 0.2] (m)
a) soda-lime-silica glass refined by sulphate
b) TV glass refined by antimony

DISCUSSION

The calculation results presented in figures 2 - 6 show a distinct influence of the redox state of glass on the interaction between glass melts and gases. The applicability of the laboratory experimental results to real conditions is therefore restricted to a case of considerable redox similarity between both situations. This is valid especially for identification of bubble sources using the experimental knowledge base of properties of laboratory modelled bubbles. However, the necessary bubble source modelling experiments in laboratory are too laborious and time consuming to be collected for more levels of the glass redox. The application of the mathematical modelling of bubbles in a glass melting space seems to be therefore a more convenient tool. At present, the truthfulness of most models is still limited by the accuracy of equilibrium and kinetic data, entering the equations of bubble behaviour. Despite that, the procedure for the bubble source identification should be prepared simultaneously with the verification of the model. This work presents the calculation procedure for the identification of air bubble source and source containing high initial concentration of CO_2 (melting bubbles) in a glass melting furnace melting soda-lime-silica glass.

The expected result of the mathematical identification system of bubble sources represents the assignment of a source and its location in the glass melting furnace to the properties of mathematically modelled bubbles, equivalent with the bubbles analysed in products. In order to be able to do this assignment, the whole melting space should be scanned for all potential bubble sources. It is necessary:

1. To define the most probable region of the given source activity in the melting space.
2. To asses the initial composition (distribution) of arisen bubbles.
3. To model behaviour of originated bubbles in a sufficient extent:

- to cover the source region by a sufficiently dense network of bubble starting points
- to model the behaviour of different initial sizes of bubbles. If $a < a_{min}$, bubble dissolves or is not formed by the source, if $a > a_{max}$, bubble is refined
- to recalculate results to ambient temperature. The recalculation involves the thermal contraction of gases, the absorption of gases by the glass melt and their eventual condensation in the bubble.

The scanning of the appropriate regions of potential bubble source should be performed for all bubble sources taken into account. The results of the scanning represents a knowledge base of the identification procedure. The bubble properties in the knowledge base are dependent from the redox, however, recalculation for another redox value is well feasible.

In table 1, the introductory part of the knowledge base valid for the air source and soda-lime-silica-glass in the model melting space is presented. All contact boundaries between the glass melt and refractory materials are defined as the potential regions of bubble source activity. The knowledge base has been calculated for the initial value of the redox $c_{oO_2} = 0.1$ mol m^{-3}.

Table 1. The introductory part of the calculated knowledge base of air bubble source in the modelling space melting soda-lime-silica glass.
a_0 (mm) - the initial bubble radius, a_b (mm) - the final bubble radius at the output temperature, a^a (mm) - the bubble radius recalculated to the ambient temperature, p^a_t (kPa) - the pressure inside of a bubble at the ambient temperature, CO_2, H_2O, N_2... (vol.%) - the volume percentage of the appropriate gas in the bubble.

bubble no.	results of bubble modelling at furnace output								results recalculated to ambient temperature				
	a_0	CO_2	H_2O	N_2	Ar	SO_2	O_2	a_b	CO_2	N_2	Ar	a^a	p^a_t
1 wall - ref. part	0.01	43.40	7.80	22.40	traces	19.69	6.71	0.30	65.96	34.04	traces	0.28	20.60
2 wall - ref. part	0.01	43.40	7.77	22.97	traces	19.53	6.33	0.27	65.39	34.61	traces	0.25	20.48
3 wall - ref. part	0.01	43.35	7.75	23.60	traces	19.34	5.96	0.24	64.75	35.25	traces	0.22	20.38
4 wall - ref. part	0.01	43.19	7.71	24.48	traces	19.12	5.50	0.21	63.83	36.17	traces	0.19	20.26
4 wall - ref. part	0.05	43.19	7.80	22.96	0.005	19.53	6.51	0.30	65.29	34.71	0.0076	0.28	20.56
4 wall - ref. part	0.10	42.92	7.84	22.43	0.017	19.73	7.06	0.38	65.65	34.32	0.0260	0.35	20.73
5 wall - ref. part	0.01	40.69	7.72	26.72	traces	18.48	6.39	0.35	60.36	39.64	traces	0.32	20.85
5 wall - ref. part	0.05	39.65	7.78	26.60	0.001	18.47	7.50	0.45	59.85	40.15	0.0015	0.42	21.37
6 wall - ref. part	0.01	41.37	7.66	27.23	traces	18.30	5.43	0.25	60.31	39.69	traces	0.23	20.49
6 wall - ref. part	0.05	40.59	7.74	26.42	0.003	18.47	6.79	0.34	60.57	39.42	0.0045	0.32	21.04
6 wall - ref. part	0.10	39.82	7.78	26.46	0.013	18.50	7.42	0.42	60.06	39.92	0.0196	0.39	21.32
6 wall - ref. part	0.15	39.07	7.82	26.66	0.025	18.43	8.00	0.51	59.41	40.55	0.0380	0.47	21.63
1 wall - melt. part	0.01	41.45	7.67	26.65	traces	18.34	5.89	0.23	60.87	39.13	traces	0.22	20.68
1 wall - melt. part	0.05	40.56	7.75	26.28	0.003	18.46	6.95	0.34	60.68	39.31	0.0045	0.32	21.11
1 wall - melt. part	0.10	39.80	7.80	26.39	0.013	18.50	7.50	0.42	60.12	39.86	0.0196	0.40	21.35
1 wall - melt. part	0.15	39.06	7.83	26.61	0.025	18.43	8.06	0.50	59.46	40.51	0.0381	0.47	21.66
2 wall - melt. part	0.01	43.05	7.74	24.57	traces	19.15	5.49	0.26	63.67	36.33	traces	0.24	20.33
2 wall - melt. part	0.05	40.07	7.82	25.34	0.001	19.07	7.70	0.50	61.25	38.74	0.0015	0.47	21.26
2 wall - melt. part	0.10	38.97	7.82	26.69	0.006	18.59	7.93	0.54	59.35	40.65	0.0091	0.50	21.54
3 wall - melt. part	0.01	40.15	7.40	30.89	0.002	17.73	3.83	0.09	56.52	43.48	0.0028	0.09	20.06

When searching for the bubble source, the results of analyses of similar bubbles are associated in one group. These results are compared with results of mathematical modelling of given bubble source. In the case the final bubble properties coincide, the appropriate starting points of mathematically modelled bubbles are designated as probable regions of bubble source in the glass melting space.

The procedure can be demonstrated by three examples. In the first one, the simulated bubble analyses provided results: c_{CO_2} (vol.%) $\in \langle 59;61 \rangle$, c_{N_2} (vol.%) $\in$ $\in \langle 35;40 \rangle$, c_{Ar} (vol.%) $\in$ $\langle$traces;0.04$\rangle$, a^a (mm) $\in$ $\in \langle 0.20;0.48 \rangle$, p^a(kPa) $\in \langle 20;22 \rangle$. Where c_i are volume concentrations of gases found by analyses, a^a is the size of analysed bubble and p^a is pressure inside of the bubble measured at ambient temperature. The results of analyses are simulated by the mathematical modelling as the agreement between experimental and calculated values is not enough sufficient yet. Nevertheless, the simulated analyses give a change to test the identification procedure. The identification procedure defined the most probable region of the air source which is presented in figure 7. As the furnace is symmetrical along the central longitudinal plane, the same region can be defined on the opposite side of the furnace. In the examined case, the probable location of the bubble source is in a small region on the wall and bottom close to the throat.

The second group of simulated analyses gave the following results: c_{CO_2} (vol.%) $\in \langle 60;65 \rangle$, c_{N_2} (vol.%) $\in$ $\in \langle 35;40 \rangle$, c_{Ar} (vol.%) $\in \langle 0.2;0.3 \rangle$, a^a (mm) $\in$ $\in \langle 0.20;0.60 \rangle$, p^a(kPa) $\in \langle 20;22 \rangle$. The results of identification procedure are obvious from figure 8. The most probable region of the air bubble source lies on the walls and bottom of the furnace working part. The extension of the region of argon concentrations to $\langle 0.01;0.3 \rangle$ extends also the probable source region into the melting part of the furnace (see the dotted region in figure 8).

In the third group of simulated bubble analyses, the batch source has been examined. The simulated analyses offered the results: c_{CO_2} (vol.%) $\in \langle 65;67 \rangle$, c_{N_2} (vol.%) $\in \langle 33;35 \rangle$, $c_{Ar} = 0$, a^a (mm) $\in \langle 0.23;0.29 \rangle$, p^a (kPa) $\in$ $\langle 20;21 \rangle$. A part of the boundary between glass batch layer and glass melt corresponding to these results of analyses is marked in figure 9.

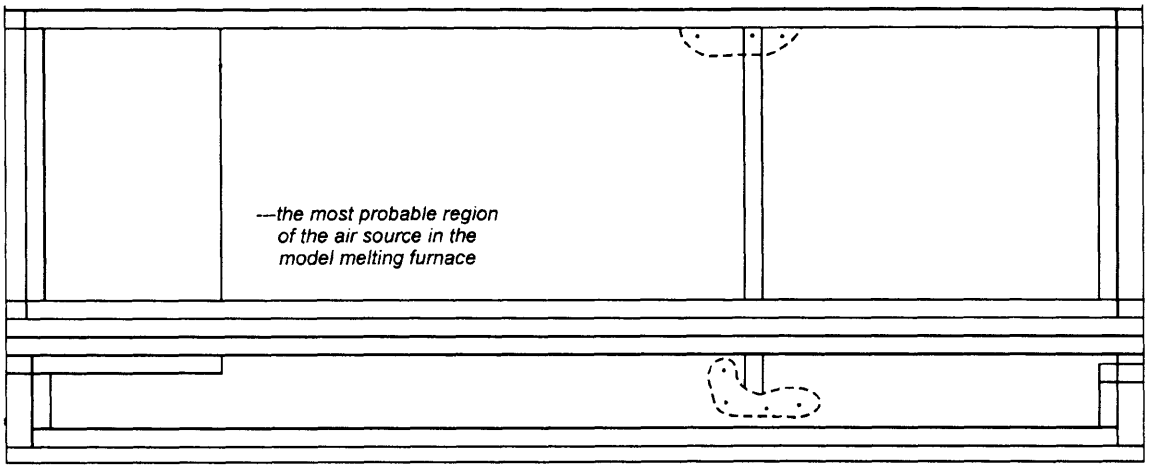

Figure 7. The probable region of the an air bubble source in the model melting furnace.
c_{CO_2} (vol.%) ∈ ⟨59;61⟩, c_{N_2} (vol.%) ∈ ⟨39;41⟩, c_{Ar} (vol.%) ∈ ⟨traces;0.04⟩, a^a (mm) ∈ ⟨0.20;0.48⟩, p^a(kPa) ∈ ⟨20;22⟩.

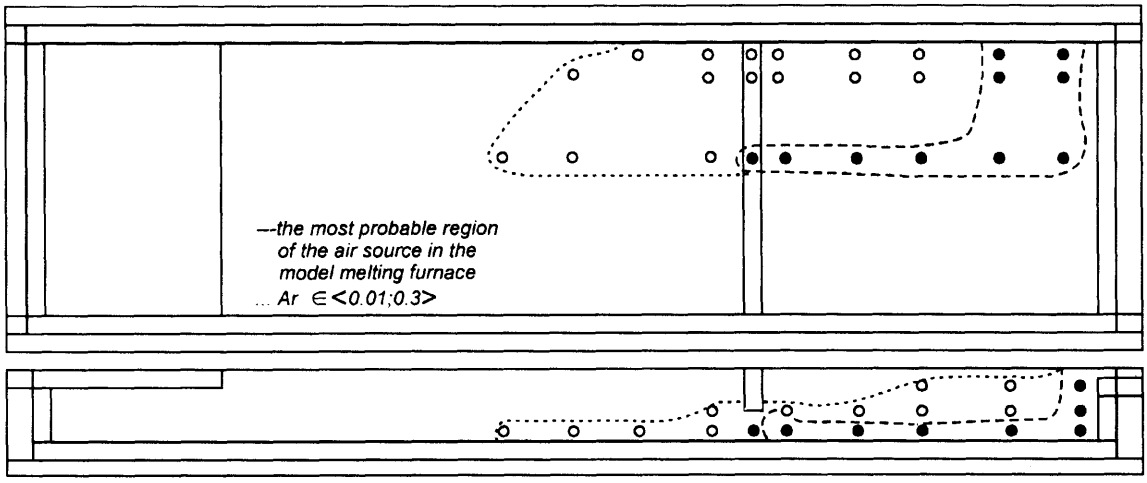

Figure 8. The probable region of an air bubble source in the model melting furnace.
c_{CO_2} (vol.%) ∈ ⟨60;65⟩, c_{N_2} (vol.%) ∈ ⟨35;40⟩, c_{Ar} (vol.%) ∈ ⟨0.01;0.3⟩, a^a (mm) ∈ ⟨0.20;0.60⟩, p^a(kPa) ∈ ⟨20;22⟩.

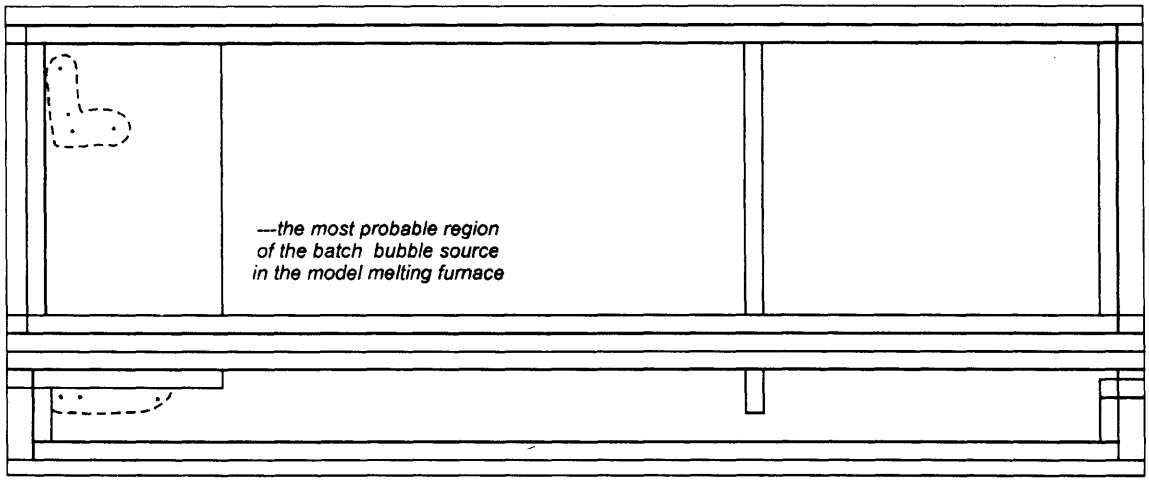

Figure 9. The probable region of the batch melting source in the model melting furnace. c_{CO2} (vol.%) ∈ ⟨65;67⟩, c_{N2} (vol.%) ∈ ⟨33;35⟩, c_{Ar} (vol.%) = 0, a^a (mm) ∈ ⟨0.23;0.29⟩, p^a(kPa) ∈ ⟨20;21⟩.

CONCLUSION

The glass melt velocity field and the oxidation-reduction field of a glass melting space are two important tools of the melting process modelling, the first one describing the hydrodynamic aspect of the process and the second the chemical interactions. Both fundamental properties are bound by the knowledge of the temperature field of the space. As is obvious, the oxidation-reduction space particularly influences the interactions between gas and glass phase. The appropriate phvsico-chemical phenomena should be therefore examined with respect to the actual oxidation-reduction state of glass. This is especially valid for the identification of bubble sources in a glass melting space using the experimental results of bubble source modelling. The restricted applicability of the experimental results of bubble modelling, valid for one level of the oxidation-reduction state of glass only, leads to a more extended application of the mathematical model which is fast and can be easily recalculated to another level of the redox. The results of simulated modelling of two bubble sources in this work show the applicability of the mathematical model of bubble behaviour for that purpose, however, the model accuracy should be heightened. The most urgent task of the near future in this field seems to be therefore the verification of the bubble model and the respective re-measuring of parameters entering the appropriate equations.

Acknowledgement

This work was supported by the grant project of The Ministry of Education, Youth and Sports of The Czech Republic No. VS 96 065.

References

1. Raková M., Němec L.: Ceramics-Silikáty *41*, 81 (1997).
2. GLASS MODEL, Mathematical model of glass melting of the company Glass Service, Ltd., Vsetín, CR.
3. Raková M.: Recherche report in the Laboratory of Inorganic Materials, ICT (1995).
4. Unpublished results of the Laboratory of Inorganic Materials.

Submitted in English by the authors.

VÝZNAM OXIDAČNĚ-REDUKČNÍHO STAVU SKEL PRO CHOVÁNÍ BUBLIN ZA NEIZOTERMNÍCH PODMÍNEK PROUDÍCÍ SKLOVINY

LUBOMÍR NĚMEC, MARKÉTA RAKOVÁ

Laboratoř anorganických materiálů,
společné pracoviště ÚACH AVČR a VŠCHT,
Technická 5, 166 28 Praha

Kombinace výpočtu simultánních oxidačně-redukčních rovnováh ve sklovině s přenosem složek oxidačně-redukčních rovnic difúzí a konvekcí skloviny poskytuje teoretický postup pro výpočet distribucí složek reakcí v reálném tavicím prostoru. Vypracovaný model spojený s rovnicemi chování vícesložkové bubliny byl použit pro zkoumání vlivu počátečního redox stavu skloviny na chování bublin. Výpočty byly aplikovány na sodno-vápenato-křemičitou sklovinu obsahující síranové ionty a ionty železa a na sklovinu pro výrobu barevných televizních obrazovek obsahující ionty antimonu a ceru. Výsledky potvrdily závěry získané za izotermních podmínek. Vnitřní parciální tlaky čeřicího plynu ve sklovině pro výrobu TV obrazovek rostly se stoupající hodnotou počátečního redox stavu skloviny (obr. 2), stejně jako rychlost procesu odstraňování bublin (obr. 4 a 5). U skla obsahujícího síranové ionty existovalo naopak minimum vnitřních parciálních tlaků SO_2 a O_2 a minimum rychlosti odstraňování bublin při středních hodnotách počáteční hodnoty redoxu (obr. 2, 4 a 5). Konečný poměr koncentrací CO_2/N_2 v bublinách vystupujících z tavicího prostoru rovněž rostl za uvedených podmínek a potvrdil závislost konečných vlastností bublin na počátečním redox stavu skloviny. Tento fakt preferuje použití teoretických modelů chování bublin při identifikaci zdrojů bublin v tavicích prostorech před modely pouze experimentálními. S použitím teoretického modelu byla získána znalostní báze vlastností bublin ze dvou zdrojů: rozkládající se vsázky a žárovzdorných materiálů pece uvolňujících vzduchové bubliny. Pomocí simulovaných analýz bublin a této báze byly pak ve třech případech lokalizovány zdroje bublin v tavicím prostoru (obr. 7 - 9).